Self-calibrated evaporation-based disaggregation of SMOS soil moisture: An evaluation study at 3 km and 100 m resolution in Catalunya, Spain

Olivier Merlin, Maria-José Escorihuela, Miquel Aran Mayoral, Olivier Hagolle, Al Bitar Ahmad, Yann H. Kerr

Self-calibrated evaporation-based disaggregation of SMOS soil moisture: an evaluation study at 3 km and 100 m resolution in Catalunya, Spain

Olivier Merlin, Maria José Escorihuela, Miquel Aran Mayoral, Olivier Hagolle, Ahmad Al Bitar, and Yann Kerr

O. Merlin is with the Centre d'Etudes Spatiales de la Biosphère (CESBIO), Toulouse, France; email: olivier.merlin@cesbio.cnes.fr

Abstract

A disaggregation algorithm is applied to 40 km resolution SMOS (Soil Moisture and Ocean Salinity) surface soil moisture using 1 km resolution MODIS (MODerature resolution Imaging Spectroradiometer), 90 m resolution ASTER (Advanced Spaceborne Thermal Emission and Reflection radiometer), and 60 m resolution Landsat-7 data. DISPATCH (DISaggregation based on Physical And Theoretical scale CHange) distributes high-resolution soil moisture around the low-resolution observed mean value using the instantaneous spatial link between optical-derived soil evaporative efficiency (ratio of actual to potential evaporation) and near-surface soil moisture. The objective is three-fold: (i) evaluating DISPATCH at a range of spatial resolutions using readily available multi-sensor thermal data, (ii) deriving a robust calibration procedure solely based on remotely sensed data, and (iii) testing the linear or nonlinear behaviour of soil evaporative efficiency. Disaggregated soil moisture is compared with the 0-5 cm in situ measurements collected each month from April to October 2011 in a 20 km square spanning an irrigated and dry

land area in Catalunya, Spain. The target downscaling resolution is set to 3 km using MODIS data and to 100 m using ASTER and Landsat data. When comparing 40 km SMOS, 3 km disaggregated and 100 m disaggregated data with the in situ measurements aggregated at corresponding resolution, results indicate that DISPATCH improves the spatio-temporal correlation with in situ measurements at both 3 km and 100 m resolutions. A yearly calibration of DISPATCH is more efficient than a daily calibration. Assuming a linear soil evaporative efficiency model is adequate at kilometric resolution. At 100 m resolution, the very high spatial variability in the irrigated area makes the linear approximation poorer. By accounting for non-linearity effects, the slope of the linear regression between disaggregated and in situ measurements is increased from 0.2 to 0.5. Such a multi-sensor remote sensing approach has potential for operational multi-resolution monitoring of surface soil moisture and is likely to help parameterize soil evaporation at integrated spatial scales.
Keywords: disaggregation, downscaling, SMOS, MODIS, ASTER, Landsat, evaporation, calibration, irrigation

1. Introduction

The current climatic trend and variability bring a questioning look to the natural supply of water resources. The point is that monitoring water resources requires observation strategies at a range of spatial scales: the atmospheric (global circulation model grid) scale, the hydrologic (catchment) scale, the administrative (irrigation area) scale and the local (field) scale. The only feasible way to provide multi-scale data sets over extended areas is through multi-sensor/multi-resolution remote sensing.

Among the variables accessible from remote sensing, soil moisture is crucial in hydrology as it controls evaporation, infiltration and runoff processes at the soil surface. However, the operational retrieval of soil moisture is currently made from passive microwave sensors at a resolution of several tens of km only. In particular, the surface soil moisture retrieved from C-band AMSR-E (Advanced Microwave Scanning Radiometer-EOS, Njoku et al. (2003)) data and L-band SMOS (Soil Moisture and Ocean Salinity, Kerr et al. (2012)) data has a spatial resolution of about 60 km and 40 km, respectively. The forthcoming SMAP (Soil Moisture Active and Passive, Entekhabi et al. (2010)) mission, scheduled for launch in 2014, will provide soil moisture data at 10 km resolution.

Optical sensors offer a wide range of spatial resolutions from several tens of meters for Landsat and ASTER (Advanced Spaceborne Thermal Emission and Reflection radiometer) to 1 km for MODIS (MODerate resolution Imaging Spectroradiometer). Although optical data have potential to monitor soil moisture, their sensitivity to other environmental factors (especially meteorological conditions and vegetation cover) makes the soil moisture retrieval impractical. Nevertheless, the synergy between low-resolution microwave and high-resolution optical data (Zhan et al., 2002) is likely to help achieve a multi-resolution soil moisture retrieval approach.

Microwave/optical data merging methods for estimating high-resolution soil moisture are generally based on the triangle (Carlson et al., 1994) or trapezoid (Moran et al., 1994) approach. Both similarly relate the variations in land surface temperature to the variations in soil water content and vegetation cover (Carlson, 2007; Petropoulos et al., 2009). In the trapezoid

approach however, the fraction of water-stressed vegetation is added as a third variable to explain a possible increase of vegetation temperature above the temperature of fully vegetated well-watered pixels.

By gathering triangle- and trapezoid-based method groups, two types of microwave/optical data merging approaches can be distinguished according to their purely-empirical (polynomial-fitting, Chauhan et al. (2003)) or semi-physical (evaporation-based, Merlin et al. (2008)) nature. The polynomial-fitting approach consists in i) expressing high-resolution soil moisture as a polynomial function of optical-derived variables (land surface temperature, vegetation index, surface albedo) available at high resolution, ii) applying the polynomial expression at low resolution to determine fitting parameters and iii) applying the polynom at high resolution using low-resolution fitted parameters. Note that the polynomial-fitting approach is rather a synergistic approach combining microwave and optical data than a disaggregation method because the conservation law is in general not satisfied at low resolution: due to the nonlinear nature of the polynomial function, the average of the estimated high-resolution soil moisture is not equal to the low-resolution observation. The evaporation-based approach uses the same optical-derived variables as the polynomial-fitting approach. However, it makes an attempt to physically represent the spatial link between optical-derived evaporation efficiency (ratio of actual to potential evaporation) and surface soil moisture. Note that other ancillary (soil and meteorological) data may be used in addition to optical data to help represent the spatio-temporal relationship between optical-derived evaporation efficiency and surface soil moisture (Merlin et al., 2008).

Piles et al. (2011) recently developed a new polynomial-fitting method by merging SMOS and MODIS data to provide surface soil moisture data at 10 km and 1 km resolution. The approach was based on Chauhan et al. (2003) except that high-resolution optical-derived surface albedo was replaced by low-resolution microwave brightness temperature in their polynomial function. The method in Piles et al. (2011) was applied to the AACES (Australian Airborne Cal/Val Experiments for SMOS, Peischl et al. (2012)) area during the SMOS commissioning phase. The polynomial coefficients were first determined at low resolution by applying the polynom to SMOS-scale brightness temperature, the MODIS land surface temperature aggregated at SMOS resolution and the MODIS-derived fraction vegetation cover aggregated at SMOS resolution. This step required to correct SMOS soil moisture product using in situ soil moisture measurements, in order to remove any bias in SMOS data. The polynomial expression was then applied at high-resolution to SMOS brightness temperature and optical data. This step required to over-sample 40 km resolution SMOS brightness temperature at 1 km resolution. Piles et al. (2011) indicated that i) introducing the low-resolution SMOS brightness temperature into the polynomial function reduced the bias between downscaled and in situ soil moisture and ii) the spatio-temporal correlation between SMOS and in situ measurements was slightly degraded when applying the polynomial-fitting method.

Kim and Hogue (2012) recently developed a new evaporation-based disaggregation (named UCLA) method of microwave soil moisture product. The approach was based on the formulation of evaporative fraction derived by Jiang and Islam (2003), and a linear scaling relationship between evapora-

tive fraction and surface soil moisture. The originality of the UCLA method relied in the representation of vegetation water stress at low resolution to derive a high-resolution soil wetness index (trapezoid approach), whilst previous evaporation-based methods assumed an unstressed vegetation cover (triangle approach). The algorithm was applied to AMSR-E level-3 soil moisture product (Njoku et al., 2003) using 1 km resolution MODIS data over the ∼75 km by 50 km SMEX04 area (Jackson et al., 2008), and the 1 km resolution disaggregated data were evaluated at the 36 SMEX sampling sites. In their paper, the authors compared the UCLA method to a range of polynomial-fitting algorithms (Chauhan et al., 2003; Hemakumara et al., 2004; Hossain and Easson, Jul. 2008) and to the evaporation-based method in Merlin et al. (2008). Results indicated that i) both evaporation-based methods (Kim and Hogue, 2012; Merlin et al., 2008) significantly improved the limited spatial variability of AMSR-E product and ii) the polynomial-fitting algorithms showed poorer performance over the SMEX04 area.

Merlin et al. (2012b) recently improved the evaporation-based method developed in Merlin et al. (2008). DISPATCH (DISaggregation based on Physical And Theoretical scale CHange) estimated high-resolution soil evaporative efficiency using high-resolution land surface temperature and NDVI data and the low-resolution temperature endmembers derived from high-resolution optical data. The link between optical data and surface soil moisture was then ensured by a nonlinear soil evaporative efficiency model, which was calibrated using available remote sensing data only. The four main improvements made in Merlin et al. (2012b) consisted in integrating a representation of: vegetation water stress at high resolution using the methodology in Moran et al.

(1994), the low-resolution sensor weighting function, the oversampling of low-resolution microwave data, and the uncertainty in output disaggregated data. DISPATCH was applied to version-4 SMOS level-2 soil moisture over the AACES area using 1 km resolution optical MODIS data, and the 1 km resolution disaggregated data were evaluated on a daily basis against 1 km resolution aggregated in situ measurements during the one-month summer and winter AACES. Results indicated a mean spatial correlation coefficient between 1 km resolution disaggregated SMOS and in situ data of about 0 during the winter AACES and 0.7-0.8 during the summer AACES.

The development of optical-based disaggregation approaches of microwave-derived soil moisture is still at its beginnings and more evaluation studies are needed. In particular, the ground data sets used to validate disaggregation methods (Chauhan et al., 2003; Piles et al., 2011; Kim and Hogue, 2012; Merlin et al., 2012b) have been limited to a one-month period although the performance of optical-based methodologies mostly relies on the atmospheric evaporative demand, which greatly varies across seasons. Also, most recent optical-based approaches have been tested using MODIS data although hydrologic and agricultural applications may require soil moisture data at a spatial resolution finer than 1 km. Last, few studies (Merlin et al., 2010c; Piles et al., 2011; Merlin et al., 2012b) have applied disaggregation approaches to SMOS soil moisture products whereas downscaling strategies may contribute to the SMOS calibration/validation by reducing the large mismatch in spatial extent between 40 km resolution SMOS observations and localized in situ measurements.

In this context, this paper seeks to (i) evaluate DISPATCH at a range

of spatial resolutions using readily available multi-sensor thermal data, (ii) derive a robust calibration procedure solely based on remotely sensed data, and (iii) test the linear or nonlinear behaviour of soil evaporative efficiency. DISPATCH is applied to last released version-5 SMOS level-2 soil moisture product over an irrigated and dry land area in Catalunya, Spain. The objective is to provide 1 km resolution surface soil moisture over a 60 km by 60 km area from 40 km resolution SMOS and 1 km resolution MODIS data and to provide 100 m resolution surface soil moisture over a 20 km by 20 km area from MODIS-disaggregated SMOS and 100 m resolution re-sampled ASTER and Landsat-7 data. Disaggregated soil moisture data are evaluated at 3 km resolution using in situ 0-5 cm measurements made once a month from April to October 2011, and at 100 m resolution using the ground data collected in August, September and October. In this study, ASTER data are considered as reference high-resolution data to evaluate the performance of DISPATCH when applied to high-quality land surface temperature data and to more operational Landsat thermal data.

The paper is organized as follows. Data sets are first described (section 2). Next, four different modes of DISPATCH are presented: the LINEAR and NONLINEAR modes (for linear or nonlinear soil evaporative efficiency model) and the DAILY and YEARLY modes (for daily or yearly calibration procedure) (section 3). Then, the linearity of soil evaporative efficiency model and its calibration procedure are tested at 3 km and 100 m resolution (section 4). Finally, an insight is given about the parameterization of soil evaporative efficiency from microwave/thermal combined remote sensing data (section 5). Last, the conclusions and perspectives are presented (section 6).

2. Data

The 60 km by 60 km study area is located east of Lleida in Catalunya, Spain. Lleida has arid continental Mediterranean climate typical of the Ebro Valley, with a mean yearly air temperature of 16°C, precipitation of 400 mm, and number of days with rain of 60. Field experiments were undertaken over a focus 20 km square area, centered on the broader 60 km study area. The 20 km square area was chosen so that it includes irrigated crops, it is relatively flat and far enough (more than 100 km) from the Pyrenees and the Mediterranean sea to limit topographic and coastal artifacts in SMOS data. It spans part of the 700 km^2 Urgell irrigation area and the surrounding dryland area, which both represent about half of the 20 km square. Irrigated crops include wheat, maize, alfalfa and fruit (apple and pear) trees while dryland crops are mainly barley, olive trees, vineyards and almond trees. An overview of the study area is presented in Figure 1.

2.1. In situ

The 0-5 cm soil moisture was measured using the gravimetric technique during seven one- (or two-) day campaigns in 2011: on DoY (Day of Year) 97-98, DoY 146-147, DoY 164-165, DoY 196, DoY 228-229, DoY 244, and DoY 277. Each field campaign was undertaken on the same sampling grid (see Figures 1c and 1d), which represented 120 soil moisture measurement (sampling) points within the 20 km square. The total sampling extent covered four 3 km by 3 km areas, with two located in the irrigated area and the other two in the dryland area. Each 3 km square was sampled by ten sampling points approximately spaced by 1 km, and three separate soil moisture

measurements were made at each sampling point. Soil texture was derived from particle size analysis at each of the 120 sampling points with a mean clay and sand fraction of 0.24 and 0.37, respectively. The approach in Saxton et al. (1986) was used to convert gravimetric measurements to volumetric values with a mean soil density estimated as 1.37 g cm^{-3}. Table 1 reports the spatial and temporal variations of 0-5 cm soil moisture obtained during the 2011 campaign in the dryland and irrigated area separately.

2.2. Remote sensing

The version-5.01 SMOS level-2 soil moisture product released on March 16, 2012 is used. Details on the processing algorithms can be found in the Algorithm Theoretical Baseline Document (ATBD, version 3.4, Kerr et al. (2011)), and on the L2SM products structure in the SMOS Level 2 and Auxiliary Data Products Specifications (SO-TN-IDR-GS-0006, Issue 6.0 2011-05-18). SMOS level-2 soil moisture data are extracted over a 100 km by 100 km area centered on the 20 km square area. Following the SMOS re-sampling strategy described in Merlin et al. (2010c), re-sampled SMOS data overlap four times over the 60 km by 60 km study area.

MODIS products MOD11A1, MYD11A1 and MOD13A2 were downloaded through the NASA Warehouse Inventory Search Tool, projected in UTM 31 North with a sampling interval of 1000 m using the MODIS reprojection tool and extracted over a 100 km by 100 km area centered on the study area, consistent with large scale SMOS data. Figure 2 presents the 1 km resolution images over the study area of Terra NDVI on DoY 225, Terra land surface temperature on DoY 228 (10:30 am) and Aqua land surface temperature on DoY 228 (1:30 pm). Some of the observed variabilities in MODIS tempera-

ture data can be attributed to vegetation cover and topographic effects.

ASTER overpassed the study area on DoY 228, DoY 244 and DoY 276 at 10:30 am local solar time. ASTER official AST_2B3 and AST_2B5 products were downloaded from ASTER Ground Data Segment Information Management System web site. ASTER 15 m resolution red (band 2) and near-infrared (band 3) bands, and ASTER 90 m resolution radiometric temperature are extracted over the 20 km square and re-sampled at 100 m resolution. NDVI is computed at 100 m resolution as the difference between near-infrared and red re-sampled bands divided by their sum. Since no cloud mask is applied to AST_2B3 and AST_2B5 products, the partially cloudy scene acquired on DoY 244 is discarded. The ASTER scenes acquired on DoY 228 and DoY 276 are cloud free. Although ASTER currently provides the best quality land surface temperature data from space, it does not acquire data continuously and data collection is scheduled upon request. Herein, ASTER data are thus considered as reference high-resolution data to evaluate the performance of DISPATCH when applied to (i) high-quality land surface temperature data and (ii) more operational Landsat data.

Landsat-7 overpassed the study area on the same dates as ASTER at around 10:30 am local solar time. Landsat level-1 radiances products were downloaded free of charge from USGS Earth Explorer website. They are available at 30 m resolution in all spectral bands. Note that the native resolution of thermal infrared bands (61 for low gain and 62 for high gain) is 60 m. In this study, Landsat level-1 visible and near-infrared bands are corrected for atmospheric effects with the algorithm in Hagolle et al. (2010), whereas thermal infrared level-1 radiances are processed without atmospheric

correction. The rationale for neglecting atmospheric effects in thermal data is based on Merlin et al. (2012b), who used the MODIS radiance-derived brightness temperature at sensor level instead of MODIS level-2 land surface temperature as input to DISPATCH. Their results indicated that correcting land surface temperature data for atmospheric effects is not a necessary step as long as the disaggregation is based on temperature differences within a 40 km size area (SMOS pixel). Herein, Landsat radiance-derived land surface temperature T is hence estimated from band 62 (high gain) by simply computing the inverse Planck function:

$$T = \frac{K_2}{\ln(\frac{K_1}{R_\lambda} + 1)} \tag{1}$$

with $K_1 = 666.09$ W m^{-2} sr^{-1} μm^{-1} and $K_2 = 1282.71$ K for band 62, and R_λ the spectral radiance in W m^{-2} sr^{-1} μm^{-1} converted from digital number (DN):

$$R_\lambda = R_{min} + (R_{max} - R_{min}) \times \frac{DN - 1}{255 - 1} \tag{2}$$

with $R_{min} = 3.20$ W m^{-2} sr^{-1} μm^{-1} and $R_{max} = 12.65$ W m^{-2} sr^{-1} μm^{-1} for band 62. Landsat-7 30 m resolution red (band 3), 30 m resolution near-infrared (band 4), and the 30 m resolution land surface temperature derived from Equation (1) are extracted over the 20 km square area and re-sampled at 100 m resolution. NDVI is computed at 100 m resolution as the difference between near-infrared and red re-sampled bands divided by their sum. The spatial extent of Landsat-7 data within the 20 km square area is delimited by the field of view, the contour of clouds detected by the algorithm in Hagolle et al. (2010) on the image acquired on DoY 244 and the data gaps (stripes)

due to Scan Line Corrector (SLC) anomaly. Since the SLC anomaly produces larger data gaps at the edge of the field of view, the processed Landsat-7 scenes are truncated at 30 km from the 183 km swath center. Figure 3 presents the 100 m resolution images over the 20 km square area of Landsat-derived NDVI and land surface temperature on DoY 228. Stripes are visible in the temperature image, but not in the NDVI image because the algorithm in Hagolle et al. (2010) interpolates shortwave data within the 60 km wide truncated Landsat-7 field of view. Note that the minimum and maximum land surface temperatures are significantly different for Landsat and ASTER data. The difference in temperature range is due mainly to atmospheric absorption (not taken into account in the derivation of Landsat temperature) and partly to the slight difference in overpass time (ASTER overpassed the study area several minutes after Landsat-7). The data coverage fraction within the 20 km square area is 82%, 57%, 94% on DoY 228, 244, 276, respectively.

3. DISPATCH

DISPATCH is an improved version of the algorithms in Merlin et al. (2008), Merlin et al. (2009), Merlin et al. (2010a) and Merlin et al. (2012b). A detailed description of DISPATCH is provided in Merlin et al. (2012b) so only the pertinent details are given here.

3.1. Linearity of soil evaporative efficiency model

One major objective of this paper is to test the linear or nonlinear behaviour of the soil evaporative efficiency model used the downscaling relationship:

$$SM = \mathbf{SM} + \left(\frac{\partial SM_{mod}}{\partial SEE}\right)_{SEE=\mathbf{SEE}} \times (SEE - \mathbf{SEE}) \quad (3)$$

with SM being the surface soil moisture disaggregated at high resolution, **SM** the low-resolution soil moisture (for clarity, the variables at coarse scale are written in bold), SEE the optical-derived soil evaporative efficiency (ratio of actual to potential evaporation), **SEE** its average within a low-resolution pixel and $\partial SM_{mod}/\partial SEE$ the partial derivative of soil moisture with respect to soil evaporative efficiency. In LINEAR mode the partial derivative in Equation (3) is computed using the simple and linear soil evaporative efficiency model in Budyko (1956) and Manabe (1969):

$$SEE_{mod} = SM/\mathbf{SM_p} \quad (4)$$

with $\mathbf{SM_p}$ being a soil parameter (in soil moisture unit). By inverting Equation (4), one obtains:

$$SM_{mod} = SEE \times \mathbf{SM_p} \quad (5)$$

Note that nonlinear soil evaporative efficiency models (Noilhan and Planton, 1989; Lee and Pielke, 1992; Komatsu, 2003) were used in the previous versions of DISPATCH (Merlin et al., 2008, 2010a, 2012b). The rationale for choosing a linear one is two-fold: (i) the model in Equation (4) may be more robust than a nonlinear model with an erroneous behaviour and (ii) it may help describe the real behaviour of soil evaporative efficiency via the calibration of $\mathbf{SM_p}$. To investigate nonlinearity effects, a NONLINEAR mode is proposed with the following soil evaporative efficiency model:

$$SEE_{mod,nl} = (SM/\mathbf{SM_{sat}})^{\mathbf{P}} \quad (6)$$

with $\mathbf{P}$ an empirical parameter and $\mathbf{SM_{sat}}$ the soil moisture at saturation. The above expression is chosen for its simplicity (it is controlled by 1 empirical parameter only), and its ability to approximately fit the exponential model in Komatsu (2003), which was successfully implemented in previous versions of DISPATCH (Merlin et al., 2008, 2010a). In addition, the model in Equation (6) equals the linear model in Equation (4) for $\mathbf{P} = 1$ and $\mathbf{SM_{sat}} = \mathbf{SM_p}$. In Equation (6), the soil moisture at saturation is estimated as in Cosby et al. (1984):

$$\mathbf{SM_{sat}} = 0.489 - 0.126 f_{sand} \quad (7)$$

with f_{sand} (-) being the sand fraction (set to 0.37). By inverting Equation (6), one obtains:

$$SM_{mod,nl} = SEE^{1/\mathbf{P}} \times \mathbf{SM_{sat}} \quad (8)$$

In NONLINEAR mode, the disaggregated soil moisture SM_{corr} is written as:

$$SM_{corr} = SM - \Delta SM_{nl} \quad (9)$$

with SM being the soil moisture disaggregated using the linear model in Equation (4) and ΔSM_{nl} a correction term:

$$\Delta SM_{nl} = SM_{mod} - SM_{mod,nl} \quad (10)$$

By replacing linear and nonlinear models by their expression in Equation (4) and (6) respectively, one obtains:

$$\Delta SM_{nl} = SEE \times \mathbf{SM_p} - SEE^{\mathbf{1/P}} \times \mathbf{SM_{sat}} \tag{11}$$

with $\mathbf{SM_p}$ and $\mathbf{P}$ being considered as fitting parameters self-estimated by DISPATCH from multi-sensor remote sensing observations.

In LINEAR mode, the soil moisture parameter $\mathbf{SM_p}$ used in Equation (4) is estimated as $\mathbf{SM/SEE}$. In NONLINEAR mode, the exponent parameter $\mathbf{P}$ used in Equation (6) is estimated as $\ln(\mathbf{SEE})/\ln(\mathbf{SM/SM_{sat}})$. By injecting calibrated $\mathbf{SM_p}$ and $\mathbf{P}$ in Equation (11), one finally obtains:

$$\Delta SM_{nl} = \frac{SEE}{\mathbf{SEE}} \times \mathbf{SM} - SEE^{\frac{\ln(\mathbf{SM/SM_{sat}})}{\ln(\mathbf{SEE})}} \times \mathbf{SM_{sat}} \tag{12}$$

Figure 4 illustrates differences between the linear and the nonlinear soil evaporative efficiency model for given values of $\mathbf{SM_p}$, $\mathbf{SM_{sat}}$, $\mathbf{SM}$ and $\mathbf{SEE}$. For each fine-scale value of SEE within the low resolution pixel, the difference between inverse soil evaporative efficiency models provide an estimate of nonlinearity effects (ΔSM_{nl} in Figure 4) on disaggregated soil moisture. Note that the nonlinear behaviour of soil evaporative efficiency is a fundamental limitation of the relationship between soil moisture and its disaggregating parameters in the higher range of soil moisture values.

3.2. Calibration procedure

Another major objective of this paper is to derive a robust calibration procedure of DISPATCH solely based on remotely sensed data.

In LINEAR mode, two different calibration strategies are tested on a daily and yearly time scale. In DAILY mode, a value of $\mathbf{SM_p}$ is obtained for each SMOS pixel and daily input data set whereas in YEARLY mode, a single value of $\mathbf{SM_p}$ is obtained for each SMOS pixel. The yearly calibration requires to run the daily calibration over the entire time series and average the daily $\mathbf{SM_p}$ for each SMOS pixel.

In NONLINEAR mode, $\mathbf{P}$ is computed daily from low-resolution $\mathbf{SM}$ and $\mathbf{SEE}$, and $\mathbf{SM_p}$ is set to the value estimated in YEARLY mode.

3.3. New version of DISPATCH

From the version described in Merlin et al. (2012b), the current version of DISPATCH differs in two main aspects: temperature endmembers are computed differently, and a correction for topographic effects is included.

3.3.1. Temperature endmembers

In the new version of DISPATCH, the minimum land surface temperature is selected among the pixels with the best land surface temperature quality index. For MODIS data, best quality is indicated by an index equal to 0. Selecting only the best quality temperature data is an efficient way to remove atmospheric effects on the MODIS pixels partly contaminated by clouds/aerosols but still retained by the MODIS algorithm for the retrieval of land surface temperature.

In Merlin et al. (2012b), the estimation of maximum vegetation temperature was constrained using additional information provided by the MODIS-derived surface albedo (Merlin et al., 2010b). Herein, a simpler approach based on fractional vegetation cover only is adopted for two reasons: (i) sur-

face albedo is not an operational product from ASTER or Landsat data and (ii) the approach in Merlin et al. (2010b, 2012b) was developed for brown agricultural soils with relatively low albedo values and may not be valid in other more heterogeneous soil conditions.

3.3.2. Topographic effects

To take into account the decrease of air temperature with altitude, a simple correction is applied to land surface temperature data:

$$T_{corr} = T + \gamma(H - \mathbf{H}) \tag{13}$$

with T_{corr} being the topography-corrected land surface temperature, T the land surface temperature derived from MODIS, ASTER or Landsat, γ (°C m^{-1}) the mean lapse rate i.e. the negative of the rate of temperature change with altitude change, H the altitude of the high-resolution optical pixel and $\mathbf{H}$ the mean altitude within the low resolution pixel. Lapse rate is set to 0.006 °C m^{-1}. Although topographic effects are expected to be low over the Urgell irrigation area, the correction in Equation (13) possibly makes disaggregation more robust in the hilly surrounding area.

4. Application

The linearity of soil evaporative efficiency model and its calibration procedure using SMOS/thermal data are tested by running DISPATCH in DAILY and YEARLY modes, and in LINEAR and NONLINEAR modes. The daily availability of MODIS data allows testing the DAILY and YEARLY modes at 3 km resolution. The high spatial resolution of ASTER/Landsat data allows

testing the LINEAR and NONLINEAR modes over the full soil moisture range. In the latter case, the low-resolution data correspond to the aggregated value within the 20 km square area of the 1 km resolution MODIS-disaggregated SMOS soil moisture obtained in YEARLY mode. In each case, DISPATCH results are compared with the in situ measurements aggregated at corresponding resolution. Note that a one-day gap between SMOS overpass and ground sampling dates is allowed in the comparison because field campaigns were made in one or two successive days.

4.1. Evaluation strategies

DISPATCH results are evaluated by two comparison strategies: the spatio-temporal comparison over the entire time series (strategy 1), and the spatial comparison at the daily time scale (strategy 2) between the remotely sensed soil moisture products and the in situ measurements aggregated at corresponding resolution.

According to strategy 1, the null-hypothesis is the temporal comparison between SMOS soil moisture and the in situ measurements aggregated at the SMOS resolution. The performance of DISPATCH is hence assessed by comparing over the entire time series the disaggregated soil moisture with the in situ measurements aggregated at corresponding resolution: 3 km for MODIS-disaggregated SMOS data and 100 m for both ASTER-disaggregated and Landsat-disaggregated SMOS data. Such a comparison between the uncertainty in SMOS data at 40 km resolution and the uncertainty in DISPATCH data at 3 km and 100 m resolution provides a useful overall assessment of the different soil moisture products.

According to strategy 2, the null-hypothesis is the UNIFORM mode of

DISPATCH defined by setting the second term of Equation (3) to zero, i.e. setting disaggregated soil moisture to SMOS soil moisture. The performance of DISPATCH is hence assessed by comparing at the daily time scale the disaggregated soil moisture with the in situ measurements aggregated at corresponding resolution: 3 km for MODIS-disaggregated SMOS data and 100 m for both ASTER-disaggregated and Landsat-disaggregated SMOS data. Such a comparison is useful to specifically evaluate the soil moisture spatial representation provided by DISPATCH at the sub-SMOS-pixel scale, by freeing from the spatio-temporal trends provided by SMOS data at 40 km resolution.

Table 2 presents the results of strategy 1 for the different application resolutions and modes of DISPATCH. At 40 km resolution, the temporal correlation between SMOS and aggregated in situ measurements is 0.59. At 3 km resolution, the spatio-temporal correlation between MODIS-disaggregated SMOS and aggregated in situ measurements is 0.67 (YEARLY mode). At 100 m resolution, the spatio-temporal correlation between ASTER-disaggregated SMOS and localized in situ measurements and between Landsat-disaggregated SMOS and localized in situ measurements is 0.73 and 0.86, respectively (LINEAR mode). Moreover, the mean difference and the root mean square difference between SMOS or disaggregated SMOS and the in situ measurements aggregated at corresponding resolution is systematically lower at 3 km and 100 m resolution than at 40 km resolution. DISPATCH thus improves the comparison between SMOS and in situ measurements. This is explained by i) the non-representativeness at the 40 km scale of the in situ measurements made in the very heterogeneous study area and ii) a relatively robust

representation of the soil moisture variability at the sub-SMOS-pixel scale.

Although strategy 1 is useful to characterize the overall spatio-temporal performance of each soil moisture product, it has several disadvantages for evaluating the soil moisture spatial representation at the sub-SMOS-pixel scale. First, strategy 1 mixes the spatio-temporal trend provided by SMOS data with the spatial trend provided by DISPATCH. Hence, separating the gain in spatial representation associated with disaggregation is nontrivial. Second, in the case where the error in disaggregation products is larger than the error in SMOS data, strategy 1 does not allow the disaggregation performance to be evaluated: disaggregation could either improve of degrade the soil moisture spatial representation at the sub-SMOS-pixel scale. Third, the statistics presented in Table 2 are not (strictly speaking) comparable. For instance, the number of data points is 15 with SMOS data and 94 with DISPATCH-Landsat data, and the range of soil moisture values is 0.02-0.18 m^3/m^3 at 40 km resolution and 0.02-0.48 m^3/m^3 at 100 m resolution.

Strategy 2 is better adapted to evaluate the soil moisture representation at the sub-SMOS-pixel scale. It allows i) comparing DISPATCH results with the null-hypothesis in the same conditions (same number of data points, and same in situ soil moisture range), ii) undertaking this comparison at the sub-SMOS-pixel scale so that the spatial trend provided by DISPATCH can be easily separated from the spatial trend provided by SMOS data at 40 km resolution and iii) undertaking this comparison at the daily time scale so that the spatial trend provided by DISPATCH can be easily separated from the temporal trend provided by SMOS data.

For the above reasons, hereafter the evaluation study of DISPATCH is

based on strategy 2 (Agam et al., 2007; Gao et al., 2012; Kim and Hogue, 2012; Merlin et al., 2010b, 2012b,a).

4.2. Testing the calibration procedure at 3 km resolution

Figures 5a, b and c plot the 3 km resolution SMOS soil moisture disaggregated in UNIFORM, DAILY and YEARLY mode as a function of aggregated in situ measurements. When comparing Figures 5a and 5b, one observes that DISPATCH provides meaningful sub-pixel information. Especially, the slope of the linear regression between disaggregated and in situ soil moisture is systematically greater than zero and close to 1 in average (see Table 3). However, data are significantly scattered around the 1:1 line. When comparing Figures 5b and 5c, one observes that the YEARLY mode is more stable than the DAILY mode. In particular, the scatter is much reduced and the slope of the linear regression between disaggregated and in situ soil moisture better stabilized at a value close to 1. Moreover, the standard deviation (represented by errorbars in Figure 5) of the downscaled soil moisture values with an estimated uncertainty greater than 0.04 m^3/m^3 is reduced by about 50% in the YEARLY mode. Hence, up to 50% of the uncertainty in downscaled soil moisture may be associated to the uncertainty in daily retrieved $\mathbf{SM_p}$. This interesting result indicates that i) retrieving $\mathbf{SM_p}$ from readily available SMOS and MODIS data is a satisfying option, ii) setting $\mathbf{SM_p}$ to a constant value improves disaggregation results, and iii) the linear approximation is well adapted at kilometric resolution.

To assess the impact of fractional vegetation cover on DISPATCH results in DAILY and YEARLY modes, Figure 5d, e and f plot the disaggregation results obtained by selecting the 1 km resolution MODIS pixels with a frac-

tional vegetatation cover lower than 0.5. Statistical results are presented in Table 4. By selecting the MODIS pixels with $f_v < 0.5$, the correlation coefficient between disaggregated and in situ soil moisture is increased from 0.6 to 0.7 and the slope of the linear regression is closer to 1. As expected, the less vegetated the surface, the more accurate soil temperature retrieval and disaggregated soil moisture. Generally speaking, optical-based disaggregation methodologies of surface soil moisture should be implemented over low-vegetated surfaces only, or by assuming that the surface soil moisture below vegetation cover is representative of mean conditions.

Note that some values of disaggregated soil moisture are negative in Figures 5c and 5f. Negative values are possible in the disaggregation output because i) DISPATCH distributes fine-scale values relatively to the mean and ii) no constraint is applied to limit the range of disaggregated values. The main advantage of keeping unphysical negative soil moisture values in output is bringing to light inconsistent $\mathbf{SM_p}$ values and/or a possible bias in SMOS data. In this study, the presence of negative values down to -0.04 m^3/m^3 is consistent with a mean difference between disaggregated and in situ soil moisture estimated as -0.06 m^3/m^3. This result is also consistent with recent and ongoing calibration/validation studies around the world, which tend to indicate a general underestimation of SMOS data with respect to 0-5 cm soil moisture measurements (Al Bitar et al., 2012; dall'Amico et al., 2012; Gherboudj et al., 2012; Sánchez et al., 2012). It is pointed out that no Radio Frequency Interference (RFI) filtering was applied to SMOS data, in order to maximize the spatio-temporal window of the comparison between disaggregated SMOS and in situ data.

Figure 6 presents the images of SMOS soil moisture and the SMOS data disaggregated at 1 km resolution in YEARLY mode for SMOS overpass on DoY 229, (a rainfall occurred on DoY 243) DoY 244, DoY 245 and DoY 277. Figure 6 also presents the images at 1 km resolution of the standard deviation of the disaggregation output ensemble.

4.3. Testing the linear approximation at 100 m resolution

Figures 7a, b and c plot the 100 m resolution SMOS soil moisture disaggregated in UNIFORM, LINEAR and NONLINEAR mode using ASTER data as a function of in situ measurements for ground data on DoY 228-229 and DoY 277. When comparing Figures 7a and 7b, one observes that DISPATCH is able to provide some sub-pixel information, but the slope of the linear regression between disaggregated and in situ data is low in LINEAR mode. When comparing Figures 7b and 7c, one observes that the NONLINEAR mode significantly improves the slope and thus the spatial representation of 100 m resolution soil moisture. The statistical results reported in Table 5 indicate that the correlation coefficient between disaggregated and in situ data is approximately the same for LINEAR and NONLINEAR modes, while the slope of the linear regression is increased from about 0.2 to 0.5 when taking into account nonlinearity effects.

Figures 7d, e and f plot the 100 m resolution SMOS soil moisture disaggregated in UNIFORM, LINEAR and NONLINEAR mode using Landsat-7 data as a function of in situ measurements for ground data on DoY 228-229, DoY 244 and DoY 277. Table 6 reports statistical results in terms of correlation coefficient, slope of the linear regression, mean difference and root mean square difference between disaggregated and in situ data. The disaggregation

results using Landsat-7 data are compared with those obtained using ASTER data. DISPATCH performances are remarkably consistent with both sensors. Slightly better results are obtained with Landsat-7 than with ASTER data, indicating that the simple derivation of land surface temperature using raw Landsat-7 thermal radiances in Equation (1) and its underlying assumptions (surface emissivity set to 1 and neglected atmospheric corrections) are appropriate for the application of DISPATCH.

Figure 8 presents the images of the SMOS data disaggregated at 100 m resolution in NONLINEAR mode using Landsat-7 (DoY 228, DoY 244 and DoY 276) and ASTER (DoY 228 and DoY 276) data and for SMOS overpasses on DoY 229, DoY 244, and DoY 277.

5. Parameterizing evaporation efficiency at integrated spatial scales

The disaggregation algorithm presented in this paper relies on the spatial link between optical-derived soil evaporative efficiency and near-surface soil moisture. If DISPATCH is able to provide reliable surface soil moisture estimates at a range of spatial resolutions, then reciprocically, one may hypothesize that the soil evaporative efficiency models used in Equation (4) and Equation (6) are reliable representations at their application scale. It is important to note however that DISPATCH also relies on the model used to estimate soil evaporative efficiency from optical data, which currently depends on soil temperature endmembers $\mathbf{T_{s,min}}$ and $\mathbf{T_{s,max}}$. In this paper, the methodology for estimating temperature endmembers is solely based on the high-resolution optical data within the low-resolution pixel, meaning that the accuracy in $\mathbf{T_{s,min}}$ and $\mathbf{T_{s,max}}$ mostly relies on the representativeness of

the surface conditions met within the low-resolution pixel. For instance, the maximum and minimum soil temperatures are expected to be biased in the case of a uniformly wet and dry SMOS pixel, respectively. An interesting point is that the representativeness of the surface conditions met within a SMOS pixel would depend on the spatial resolution of optical data. In particular, the temperature range of land surface temperature is different for MODIS and ASTER data (not shown) although they are associated with the same surface conditions. Irrigated areas including both dry mature and early stage wet crops (and possibly water reservoirs) do provide the heterogeneous conditions to estimate temperature endmembers accurately, as long as the spatial resolution of the optical sensors is finer than the typical field size. Consequently, the application of DISPATCH with 1 km resolution MODIS data on one side and with 100 m resolution Landsat or ASTER data on the other may require different soil evaporative efficiency representations due to the lack of transferability across resolutions of the methodology used for estimating temperature end-members.

The meaningfulness of the linear soil evaporative efficiency model in Equation (4) is investigated by plotting in Figure 9a the MODIS-derived soil evaporative efficiency aggregated at 40 km resolution as a function of SMOS soil moisture for the entire time series from April to October 2011. While the slope of the linear regression between aggregated MODIS-derived soil evaporative efficiency and SMOS soil moisture is positive, no significant correlation is observed. The non-uniqueness of the relationship between soil evaporative efficiency and surface soil moisture in changing atmospheric conditions has been reported in a number of studies (Chanzy and Bruckler, 1993; Merlin

et al., 2011). However, the SMOS-scale soil evaporative efficiency seems to be quasi constantly equal to 0.5, which is not consistent with the great soil moisture range covered by SMOS data. To further investigate the particular behaviour of aggregated MODIS-derived soil evaporative efficiency, the daily retrieved $\mathbf{SM_p}$ parameter is plotted in Figure 9b as a function of SMOS soil moisture. A strong correlation is visible with a slope of the linear regression between $\mathbf{SM_p}$ and SMOS soil moisture of about 2. Both results ($\mathbf{SEE} \sim 0.5$ and $\mathbf{SM_p/SM} \sim 2$) tend to indicate that there is a significant compensation effect between **SEE** and $\mathbf{SM_p}$ variations. It is thus highly probable that the daily variations in retrieved $\mathbf{SM_p}$ be partly due to the variations in **SEE** associated with biased estimates of temperature endmembers $\mathbf{T_{s,min}}$ and $\mathbf{T_{s,max}}$.

The above discussion hypothesizes that a robust spatio-temporal estimation of temperature end-members $\mathbf{T_{s,min}}$ and $\mathbf{T_{s,max}}$ would help parameterizing soil evaporative efficiency at a range of spatial scales. Future studies may use a soil energy balance model to simulate the minimum and maximum soil temperatures with a better accuracy than using the methodology solely based on remote sensing optical data. This would require meteorological data composed of air temperature, solar radiation, wind speed and relative humidity at a 40 km resolution or finer. Note that in this case, DISPATCH would no longer operate with relative values since the algorithm would combine remotely sensed temperature with the temperature endmembers estimated from other ancillary data. Consequently, remotely sensed temperature data should be fully compatible with those simulated by the energy balance model. In particular, the simple approach used in the paper to estimate land surface

temperature from raw Landsat thermal radiances would no longer be valid when using an energy balance model.

6. Conclusion

In this study, DISPATCH is applied to 40 km resolution SMOS soil moisture data over an irrigated and dry land area in Catalunya, Spain. The objective is to provide 1 km resolution surface soil moisture over a 60 km 60 km area from SMOS and 1 km resolution MODIS data and to provide 100 m resolution surface soil moisture over a 20 km by 20 km area from MODIS-disaggregated SMOS and 100 m resolution Landsat and ASTER data. Disaggregated soil moisture data are evaluated at 3 km resolution using in situ 0-5 cm measurements made once a month from April to October 2011, and at 100 m resolution using the ground data collected in August, September and October.

To investigate the overall spatio-temporal performance of DISPATCH soil moisture products, a first comparison is conducted over the entire time series. At 40 km resolution, the temporal correlation between SMOS and aggregated in situ measurements is 0.59. At 3 km resolution, the spatio-temporal correlation between MODIS-disaggregated SMOS and aggregated in situ measurements is 0.67. At 100 m resolution, the spatio-temporal correlation between ASTER-disaggregated SMOS and localized in situ measurements and between Landsat-disaggregated SMOS and localized in situ measurements is 0.73 and 0.86, respectively. Moreover, the mean difference and the root mean square difference between SMOS or disaggregated SMOS and the in situ measurements aggregated at corresponding resolution is sys-

tematically lower at 3 km and 100 m resolution than at 40 km resolution. DISPATCH thus improves the comparison between SMOS and in situ measurements. This is explained by i) the non-representativeness at the 40 km scale of the in situ measurements made in the very heterogeneous study area and ii) a relatively robust representation of soil moisture variability at the sub-SMOS-pixel scale.

To specifically investigate the soil moisture spatial representation at the sub-SMOS-pixel scale, a second comparison is conducted at the daily time scale. At 3 km resolution, results indicate that (i) the mean daily correlation coefficient and the mean daily slope of the linear regression between disaggregated and in situ data is 0.7 and 0.8 respectively, (ii) a yearly calibration of the soil evaporative efficiency model makes the algorithm more robust with a greater stability of the slope around 1, and (iii) assuming a linear soil evaporative efficiency model is adequate at kilometric resolution. At 100 m resolution, results indicate with both Landsat and ASTER data a mean daily correlation coefficient between disaggregated SMOS and in situ data of about 0.7 but a low slope of the mean daily linear regression estimated as 0.2. When adding a correction for non-linearity effects between soil evaporative efficiency and surface soil moisture, the mean daily correlation coefficient between disaggregated SMOS and in situ data is kept relatively constant while the slope of the mean daily linear regression is improved from 0.2 to about 0.5.

If DISPATCH is able to provide reliable surface soil moisture estimates at a range of spatial resolutions, then reciprocally, one may hypothesize that the soil evaporative efficiency model used in the algorithm is a reliable represen-

tation at the application scale. However, compensation effects are identified between optical-derived soil evaporative efficiency and the retrieved soil evaporative efficiency parameter. These compensation effects are attributed to the methodology for estimating temperature endmembers solely based on remote sensing data. DISPATCH could be a useful tool to help parameterize soil evaporative efficiency at a range of spatial scales, but to do so, independent meteorological data should be used to better constrain the temperature endmembers in both space and time.

This study demonstrates the potential of DISPATCH for operational multi-scale monitoring of surface soil moisture using readily available SMOS, MODIS and Landsat/ASTER data. Due to the recent failure of Landsat-5, the provision of high-resolution thermal data currently relies on on-request ASTER and SLC-off Landsat-7 data. The Landsat Data Continuity Mission (LDCM), with increased coverage capabilities, is scheduled for launch in 2013. In the medium term, the continuity of L-band derived soil moisture data will be ensured by the SMAP mission, scheduled for launch in 2014.

Acknowledgements

Project RD10-1-0035 co-financed by the European Regional Development Fund under the Catalan operational program 2007-2013.

References

Agam, N., Kustas, W. P., Anderson, M. C., Li, F., Neale, C. M. U., 2007. A vegetation index based technique for spatial sharpening of thermal imagery. Remote Sens. Environ. 107, 545–558.

669 Al Bitar, A., Leroux, D., Kerr, Y. H., Merlin, O., Richaume, P., Sahoo,
670 A., Wood, E. F., 2012. Evaluation of SMOS soil moisture products over
671 continenal U.S. using the SCAN/SNOTEL network. IEEE Trans. Geosci.
672 Remote Sens. 50 (5), 1572–1586, doi:10.1109/TGRS.2012.2186581.

673 Budyko, M. I., 1956. Heat balance of the Earth's surface. Gidrometeoizdat,
674 Leningrad.

675 Carlson, T., 2007. An overview of the 'triangle method' for estimating sur-
676 face evapotranspiration and soil moisture from satellite imagery. Sensors
677 7, 1612–1629.

678 Carlson, T. N., Gillies, R. R., Perry, E. M., 1994. A method to make use of
679 thermal infrared temperature and NDVI measurements to infer soil water
680 content and fractional vegetation cover. Remote Sens. Rev. 52, 45–59.

681 Chanzy, A., Bruckler, L., 1993. Significance of soil surface moisture with
682 respect to daily bare soil evaporation. Water Resour. Res. 29 (4), 1113–
683 1125.

684 Chauhan, N. S., Miller, S., Ardanuy, P., 2003. Spaceborne soil moisture es-
685 timation at high resolution: a microwave-optical/IR synergistic approach.
686 Int. J. Remote Sens. 24 (22), 4599–4622.

687 Cosby, B. J., Hornberger, G. M., Clapp, R. B., Ginn, T. R., 1984. A statis-
688 tical exploration of the relationships of soil moisture characteristics to the
689 physical properties of soils. Water Resour. Res. 20, 682–690.

690 dall'Amico, J. T., Schlenz, F., Loew, A., Mauser, W., 2012. First
691 results of SMOS soil moisture validation in the upper Danube

692 catchment. IEEE Trans. Geosci. Remote Sens. 50 (5), 1507–1516,
693 doi:10.1109/TGRS.2011.2171496.

694 Entekhabi, D., Njoku, E. G., O'Neill, P. E., Kellogg, K. H., Crow, W. T.,
695 Edelstein, W. N., Entin, J. K., Goodman, S. D., Jackson, T. J., Johnson,
696 J., Kimball, J., Piepmeier, J. R., Koster, R., Martin, N., McDonald, K. C.,
697 Moghaddam, M., Moran, S., Reichle, R., Shi, J. C., Spencer, M. W.,
698 Thurman, S. W., Tsang, L., Van Zyl, J., 2010. The Soil Moisture Active
699 Passive (SMAP) mission. Proceedings of the IEEE 98 (5), 704–716.

700 Gao, F., Kustas, W. P., Anderson, M. C., 2012. A data mining approach
701 for sharpening thermal satellite imagery over land. Remote Sens. 4, 3287–
702 3319, doi:10.3390/rs4113287.

703 Gherboudj, I., Magagi, R., Goita, K., Berg, A. A., Toth, B., Walker, A.,
704 2012. Validation of SMOS data over agricultural and boreal forest ar-
705 eas in Canada. IEEE Trans. Geosci. Remote Sens. 50 (5), 1623–1635,
706 doi:10.1109/TGRS.2012.2188532.

707 Hagolle, O., Huc, M., Pascual, D. V., Dedieu, G., 2010. A multi-temporal
708 method for cloud detection, applied to FORMOSAT-2, VENuS, LAND-
709 SAT and SENTINEL-2 images. Remote Sens. Environ. 114 (8), 1747–1755,
710 doi:10.1016/j.rse.2010.03.002.

711 Hemakumara, H. M., Kalma, J. D., Walker, J. P., Willgoose, G. R., 2004.
712 Downscaling of low resolution passive microwave soil moisture observa-
713 tions. In: Proc. 2nd Int. CAHMDA Workshop Terrestrial Water Cycle.
714 Princeton, NJ, pp. 67–73.

715 Hossain, A., Easson, G., Jul. 2008. Evaluating the potential of VI-LST tri-
716 angle model for quantitative estimation of soil moisture using optical im-
717 agery. In: Proc. IEEE Int. Geosci. Remote Sens. Symp. Boston, MA, pp.
718 III879–III882.

719 Jackson, T. J., Moran, M. S., O'Neill, P. E., 2008. Introduction to Soil Mois-
720 ture EXperiments 2004 (SMEX04). Remote Sens. of Environ. 112 (2), 301–
721 303.

722 Jiang, L., Islam, S., 2003. An intercomparison of regional latent heat flux
723 estimation using remote sensing data. Int. J. Remote Sens. 24, 2221–2236.

724 Kerr, Y. H., Waldteufel, P., Richaume, P., Ferrazzoli, P., Wigneron, J.-P.,
725 2011. SMOS level 2 processor soil moisture Algorithm Theoretical Ba-
726 sis Document (ATBD). Vol. SO-TN-ESL-SM-GS-0001, V3.4. CESBIO,
727 Toulouse, France.

728 Kerr, Y. H., Waldteufel, P., Richaume, P., Wigneron, J. P., Ferrazzoli, P.,
729 Mahmoodi, A., Al Bitar, A., Cabot, F., Gruhier, C., Leroux, D., Mialon,
730 A., Delwart, S., 2012. The SMOS soil moisture retrieval algorithm. IEEE
731 Trans. Geosci. Remote Sens.Doi:10.1109/TGRS.2012.2184548.

732 Kim, J., Hogue, T. S., 2012. Improving spatial soil moisture representa-
733 tion through integration of AMSR-E and MODIS products. IEEE Trans.
734 Geosci. Remote Sens. 50 (2), 446–460, doi:10.1109/TGRS.2011.2161318.

735 Komatsu, T. S., 2003. Towards a robust phenomenological expression of evap-
736 oration efficiency for unsaturated soil surfaces. J. Appl. Meteorol. 42, 1330–
737 1334.

738 Lee, T. J., Pielke, R. A., 1992. Estimating the soil surface specific humidity.
739 J. Appl. Meteor. 31, 480–484.

740 Manabe, S., 1969. Climate and the ocean circulation. I. The atmospheric
741 circulation and the hydrology of the Earth's surface. Month. Weather Rev.
742 97 (11), 739–774.

743 Merlin, O., Al Bitar, A., Rivalland, V., Béziat, P., Ceschia, E., Dedieu, G.,
744 2011. An analytical model of evaporation efficiency for unsaturated soil
745 surfaces with an arbitrary thickness. J. Appl. Meteor. Clim. 50 (2), 457–
746 471, doi:10.1175/2010JAMC2418.1.

747 Merlin, O., Al Bitar, A., Walker, J. P., Kerr, Y., 2009. A sequential model
748 for disaggregating near-surface soil moisture observations using multi-
749 resolution thermal sensors. Remote Sens. Environ. 113 (10), 2275–2284,
750 doi:10.1016/j.rse.2009.06.012.

751 Merlin, O., Al Bitar, A., Walker, J. P., Kerr, Y., 2010a. An improved al-
752 gorithm for disaggregating microwave-derived soil moisture based on red,
753 near-infrared and thermal-infrared data. Remote Sens. Environ. 114 (10),
754 2305–2316, doi:10.1016/j.rse.2010.05.007.

755 Merlin, O., Duchemin, B., Hagolle, O., Jacob, F., Coudert, B., Chehbouni,
756 G., Dedieu, G., Garatuza, J., Kerr, Y., 2010b. Disaggregation of MODIS
757 Surface Temperature over an Agricultural Area Using a Time Series
758 of Formosat-2 Images. Remote Sens. Environ. 114 (11), 2500–2512,
759 doi:10.1016/j.rse.2010.05.025.

760 Merlin, O., Jacob, F., Wigneron, J.-P., Walker, J., Chehbouni, G.,
761 2012a. Multidimensional disaggregation of land surface temperature us-
762 ing high-resolution red, near-infrared, shortwave-infrared, and microwave-
763 L bands. IEEE Trans. Geosci. Remote Sens. 50 (5), 1864–1880,
764 doi:10.1109/TGRS.2011.2169802.

765 Merlin, O., Rüdiger, C., Al Bitar, A., Richaume, P., Walker, J. P.,
766 Kerr, Y. H., 2012b. Disaggregation of SMOS soil moisture in South-
767 eastern Australia. IEEE Trans. Geosci. Remote Sens. 50 (5), 1557–1571,
768 doi:10.1109/TGRS.2011.2175000.

769 Merlin, O., Rüdiger, C., Richaume, P., Al Bitar, A., Mialon, A., Walker, J. P.,
770 Kerr, Y., 2010c. Disaggregation as a top-down approach for evaluating 40
771 km resolution SMOS data using point-scale measurements: application
772 to AACES-1. In: SPIE, Remote Sensing of Agriculture, Ecosystems, and
773 Hydrology XII. Toulouse, France, pp. 78240I–1–8, doi:10.1117/12.865751.

774 Merlin, O., Walker, J. P., Chehbouni, A., Kerr, Y., 2008. Towards
775 deterministic downscaling of SMOS soil moisture using MODIS de-
776 rived soil evaporative efficiency. Remote Sens. Environ. 112, 3935–3946,
777 doi:10.1016/j.rse.2008.06.012.

778 Moran, M. S., Clarke, T. R., Inoue, Y., Vidal, A., 1994. Estimating crop wa-
779 ter deficit using the relation between surface-air temperature and spectral
780 vegetation index. Remote Sens. Environ. 49, 246–263.

781 Njoku, E., Jackson, T., Lakshmi, V., Chan, T., Nghiem, S., 2003. Soil mois-

ture retrieval from AMSR-E. IEEE Trans. Geosci. Remote Sens. 41, 215–229.

Noilhan, J., Planton, S., 1989. A simple parameterization of land surface processes for meteorological models. Mon. Wea. Rev. 117, 536–549.

Peischl, S., Walker, J. P., Ye, C. R. N., Kerr, Y. H., Kim, E., Bandara, R., Allahmoradi, M., 2012. The AACES field experiments: SMOS calibration and validation across the Murrumbidgee river catchment. Hydrol. Earth Sci. Discuss. 9, 2763–2795, doi:10.5194/hessd-9-2763-2012.

Petropoulos, G., Carlson, T., Wooster, M., Islam, S., 2009. A review of Ts/VI remote sensing based methods for the retrieval of land surface energy fluxes and soil surface moisture. Prog. Phys. Geography 33 (2), 224–250.

Piles, M., Camps, A., Vall-llossera, M., Corbella, I., Panciera, R., Rüdiger, C., Kerr, Y. H., Walker, J. P., 2011. Downscaling SMOS-derived soil moisture using MODIS visible/infrared data. IEEE Trans. Geosci. and Remote Sens. 49 (9), 3156–3166, doi:10.1109/TGRS.2011.2120615.

Sánchez, N., Martínez-Fernández, J., Pérez-Gutiérrez, C., 2012. Validation of the SMOS L2 soil moisture data in the REMEDHUS network (Spain). IEEE Trans. Geosci. Remote Sens. 50 (5), 1602–1611, doi:10.1109/TGRS.2012.2186971.

Saxton, K. E., Rawls, W. J., Romberger, J. S., Papendick, R. I., 1986. Estimating Generalized Soil-water Characteristics from Texture. Soil Sci. Soc. Amer. J. 50 (4), 1031–1036.

804 Zhan, X., Miller, S., Chauhan, N., Di, L., Ardanuy, P., 2002. Soil mois-
805 ture visible/infrared radiometer suite algorithm theoretical basis docu-
806 ment. Vol. Tech. Rep. Raytheon Syst. Company, Lanham, MD.

Table 1: Mean and standard deviation (std) of 0-5 cm deep in situ soil moisture measurements. Results are presented for each field campaign, and over the dryland and irrigated area separately.

Month	Dryland area Mean (std) m^3/m^3	Irrigated area Mean (std) m^3/m^3
Apr	0.012 (0.002)	0.017 (0.003)
May	0.075 (0.025)	0.10 (0.078)
Jun	0.12 (0.051)	0.19 (0.073)
Jul	0.081 (0.029)	0.15 (0.085)
Aug	0.021 (0.006)	0.16 (0.072)
Sep	- (-)	0.23 (0.047)
Oct	0.032 (0.017)	0.066 (0.027)

Table 2: Correlation coefficient (R), slope of the linear regression, mean difference (bias) and root mean square difference (RMSD) between SMOS or DISPATCH SM and the in situ measurements aggregated at corresponding resolution: 40 km for SMOS SM, 3 km for MODIS-disaggregated SMOS SM, and 100 m resolution for ASTER- and Landsat-disaggregated SMOS SM. The number of data points and the minimum and maximum values of aggregated in situ measurements are also reported.

Data	Spatial resolution	Thermal data	DISPATCH mode	R (-)	Slope (-)	Bias (m^3/m^3)	RMSD (m^3/m^3)	Number of data points	In situ SM range (m^3/m^3)
SMOS	40 km	none	none	0.59	0.25	−0.099	0.12	15	0.02-0.18
DISPATCH	3 km	MODIS	DAILY	0.58	0.46	−0.077	0.11	54	0.02-0.32
DISPATCH	3 km	MODIS	YEARLY	0.67	0.40	−0.084	0.11	54	0.02-0.32
DISPATCH	100 m	ASTER	LINEAR	0.73	0.18	−0.049	0.090	79	0.02-0.48
DISPATCH	100 m	Landsat	LINEAR	0.86	0.32	−0.068	0.11	94	0.02-0.48
DISPATCH	100 m	ASTER	NONLINEAR	0.69	0.50	−0.031	0.073	79	0.02-0.48
DISPATCH	100 m	Landsat	NONLINEAR	0.83	0.48	−0.052	0.090	94	0.02-0.48

Table 3: Mean (and standard deviation of) daily correlation coefficient (R), slope of the linear regression, mean difference (bias) and root mean square difference (RMSD) between disaggregated SMOS SM and in situ measurements aggregated at 3 km resolution. Comparison results are presented for all the 1 km MODIS pixels.

Mode	R (-)	Slope (-)	Bias (m^3/m^3)	RMSD (m^3/m^3)
UNIFORM	0.34 (0.55)	0.01 (0.02)	−0.11 (0.038)	0.12 (0.039)
DAILY	0.61 (0.33)	0.73 (0.96)	−0.071 (0.059)	0.093 (0.046)
YEARLY	0.61 (0.32)	0.58 (0.45)	−0.079 (0.055)	0.092 (0.047)

Table 4: Mean (and standard deviation of) daily correlation coefficient (R), slope of the linear regression, mean difference (bias) and root mean square difference (RMSD) between disaggregated SMOS SM and in situ measurements aggregated at 3 km resolution. Comparison results are presented for the 1 km MODIS pixels with a fractional vegetation cover lower than 0.5.

Mode	R (-)	Slope (-)	Bias (m^3/m^3)	RMSD (m^3/m^3)
UNIFORM	−0.07 (0.60)	0.01 (0.03)	−0.081 (0.057)	0.093 (0.051)
DAILY	0.70 (0.32)	0.86 (0.70)	−0.057 (0.052)	0.078 (0.036)
YEARLY	0.71 (0.32)	0.78 (0.31)	−0.067 (0.050)	0.079 (0.038)

Table 5: Daily correlation coefficient (R), slope of the linear regression, mean difference (bias) and root mean square difference (RMSD) between the SMOS SM disaggregated at 100 m resolution using ASTER data and localized in situ measurements. Comparison results are presented for each SMOS overpass date separately: DoY 229, DoY 244, DoY 277.

Mode	R (-)	Slope (-)	Bias (m^3/m^3)	RMSD (m^3/m^3)
UNIFORM	0.00, -, 0.00	0.00, -, 0.00	−0.071, -, −0.029	0.14, -, 0.047
LINEAR	0.80, -, 0.42	0.18, -, 0.20	−0.070, -, −0.029	0.12, -, 0.045
NONLINEAR	0.77, -, 0.37	0.51, -, 0.48	−0.045, -, −0.017	0.089, -,0.053

Table 6: Daily correlation coefficient (R), slope of the linear regression, mean difference (bias) and root mean square difference (RMSD) between the SMOS SM disaggregated at 100 m resolution using Landsat-7 data and localized in situ measurements. Comparison results are presented for each SMOS overpass date separately: DoY 229, DoY 244, DoY 277.

Mode	R (-)	Slope (-)	Bias (m^3/m^3)	RMSD (m^3/m^3)
UNIFORM	0.00, 0.00, 0.00	0.00, 0.00, 0.00	−0.069, −0.18, −0.029	0.14, 0.19, 0.047
LINEAR	0.81, 0.40, 0.60	0.16, 0.073, 0.28	−0.068, −0.17, −0.028	0.12, 0.17, 0.041
NONLINEAR	0.80, 0.40, 0.55	0.43, 0.26, 0.65	−0.054, −0.14, −0.017	0.095, 0.15, 0.043

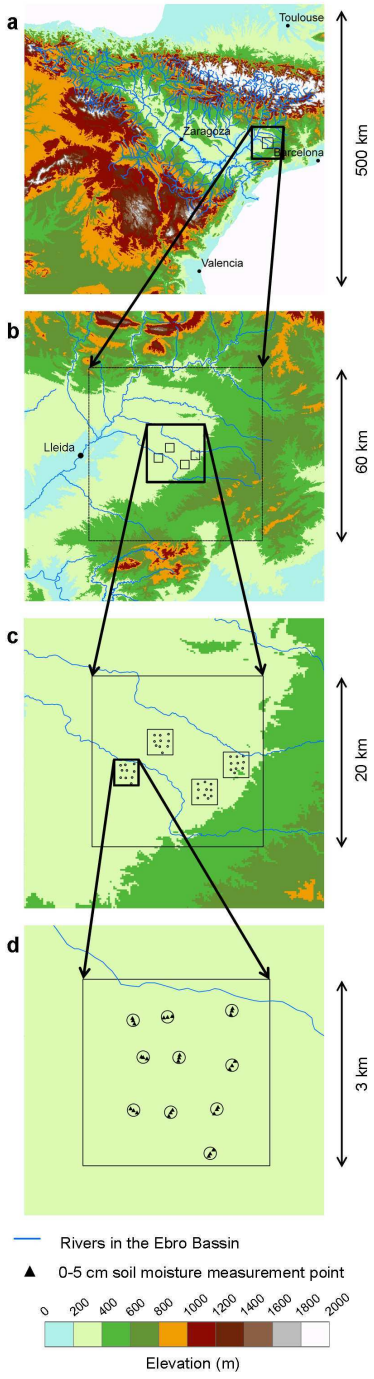

Figure 1: Overview of the study area and the ground sampling strategy.

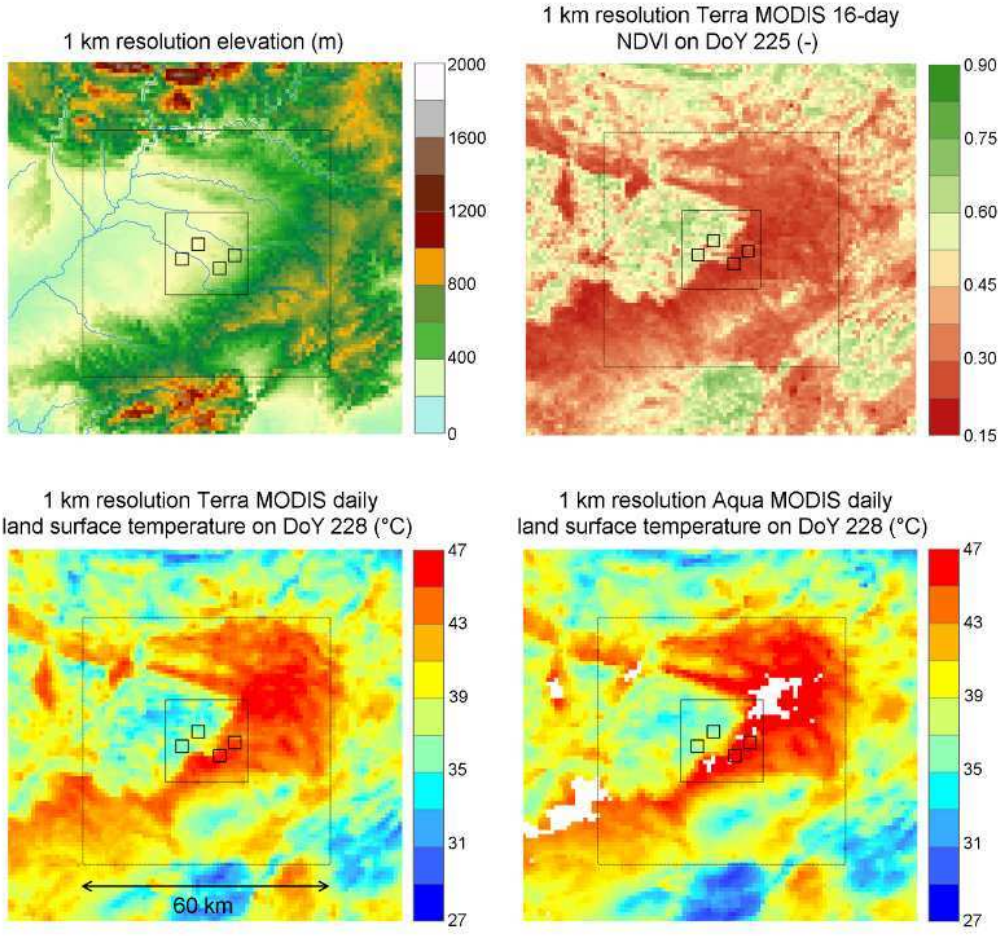

Figure 2: Images at 1 km resolution of elevation, Terra MODIS NDVI on Doy 225, Terra MODIS land surface temperature on DoY 228 (10:30 am) and Aqua MODIS land surface temperature on DoY 228 (1:30 pm).

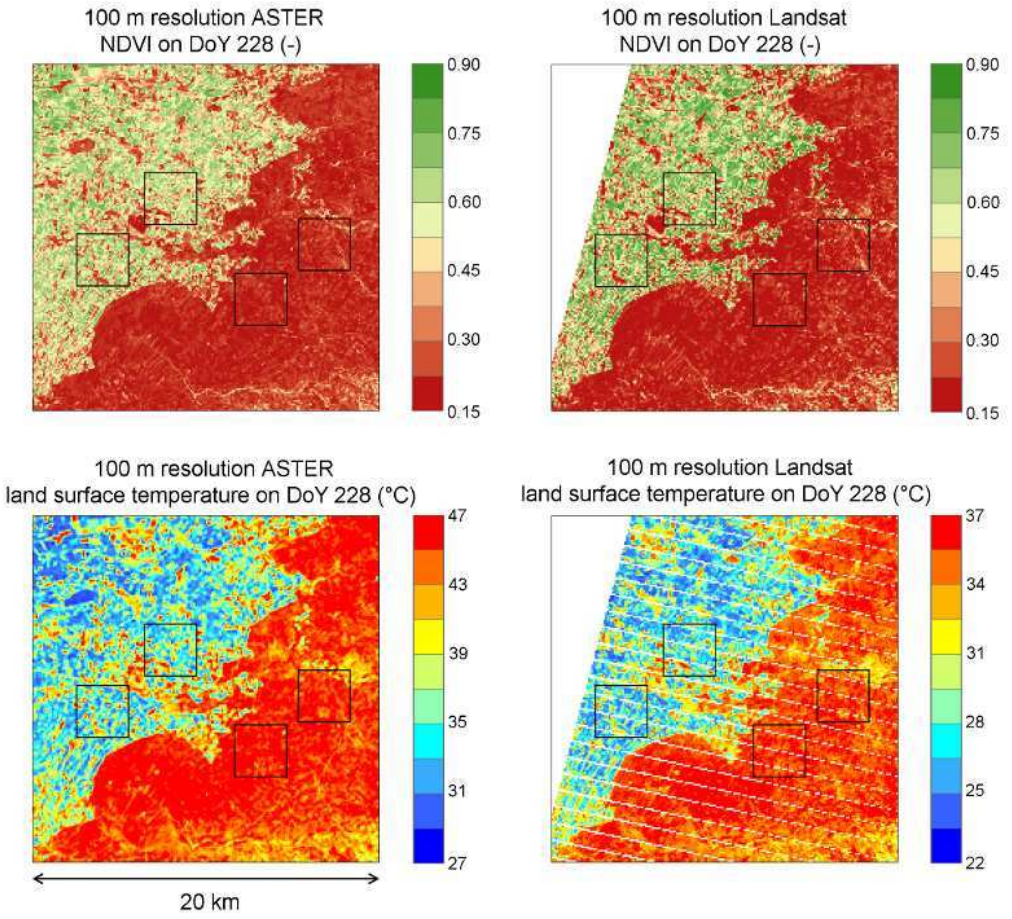

Figure 3: Images at 100 m resolution over the 20 km square area of ASTER- and Landsat-derived NDVI, and land surface temperature on DoY 228.

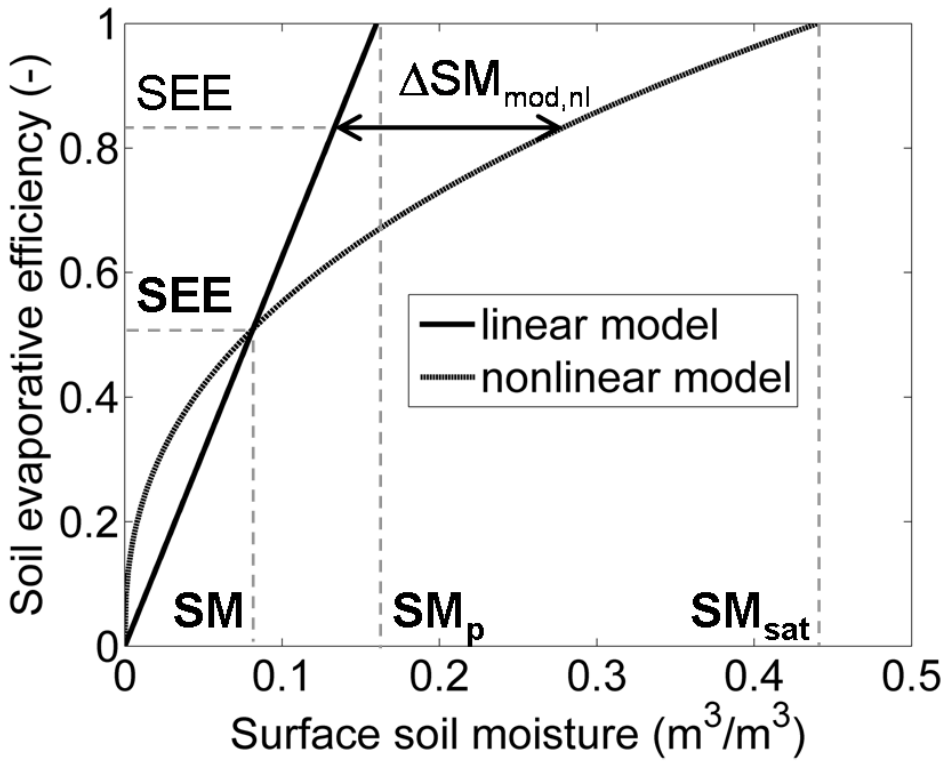

Figure 4: Soil evaporative efficiency modelled by the linear and nonlinear model versus surface soil moisture. The difference between inverse models is used to correct disaggregation output for nonlinearity effects.

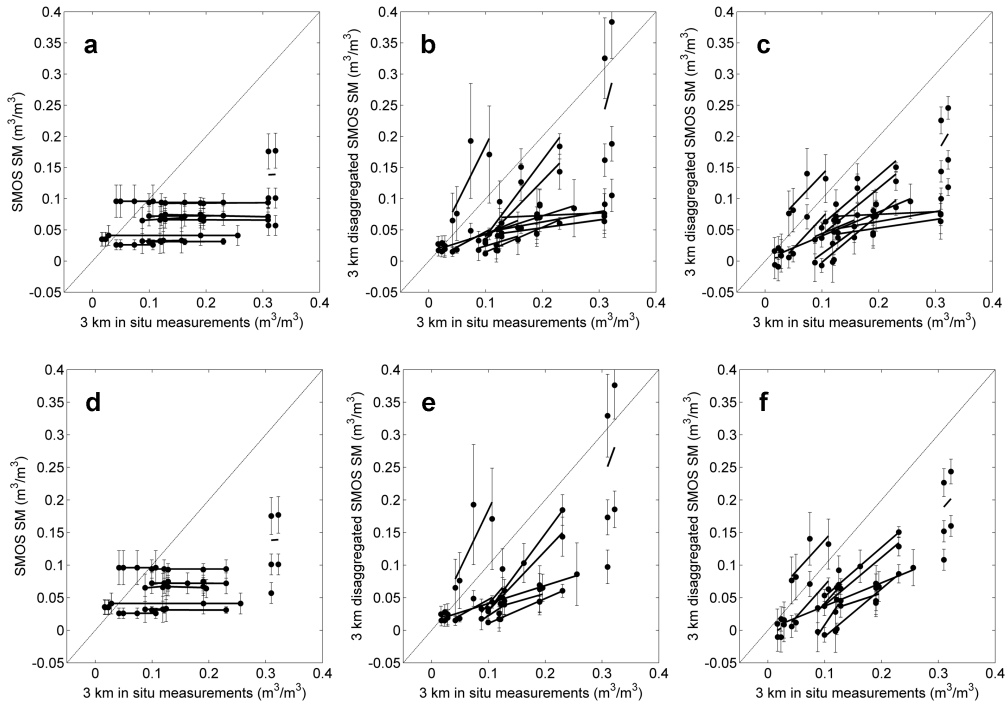

Figure 5: The SMOS soil moisture disaggregated in the UNIFORM (a and d), DAILY (b and e) and YEARLY (c and f) mode is plotted as a function of in situ measurements aggregated at 3 km resolution for all the MODIS pixels (top), and for the MODIS pixels with $f_v < 0.5$ (bottom). Errorbars represent the standard deviation of disaggregation output ensemble for each 3 km by 3 km ground sampling area, and the segments are the linear fit of daily data.

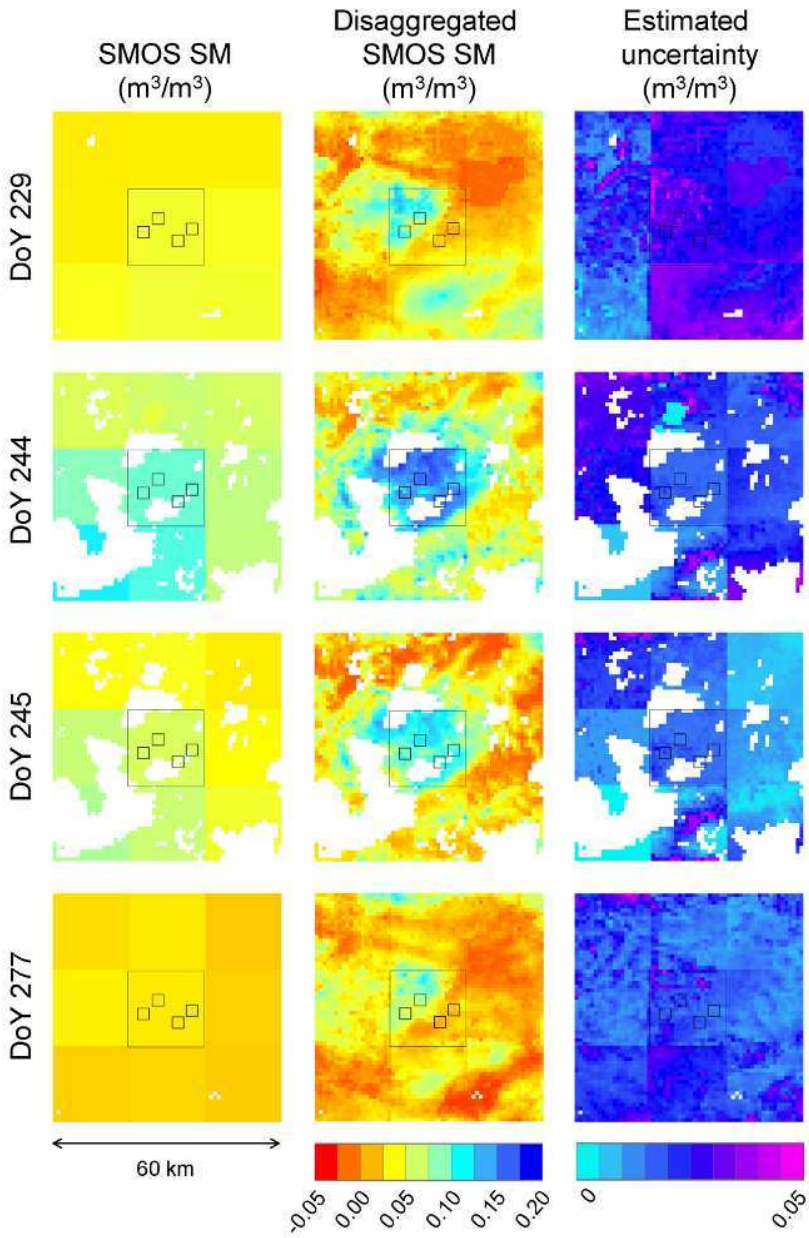

Figure 6: Images of SMOS soil moisture, the SMOS data disaggregated at 1 km resolution in YEARLY mode, and the estimated uncertainty in disaggregated data for SMOS overpass on DoY 229, DoY 244, DoY 245 and DoY 277.

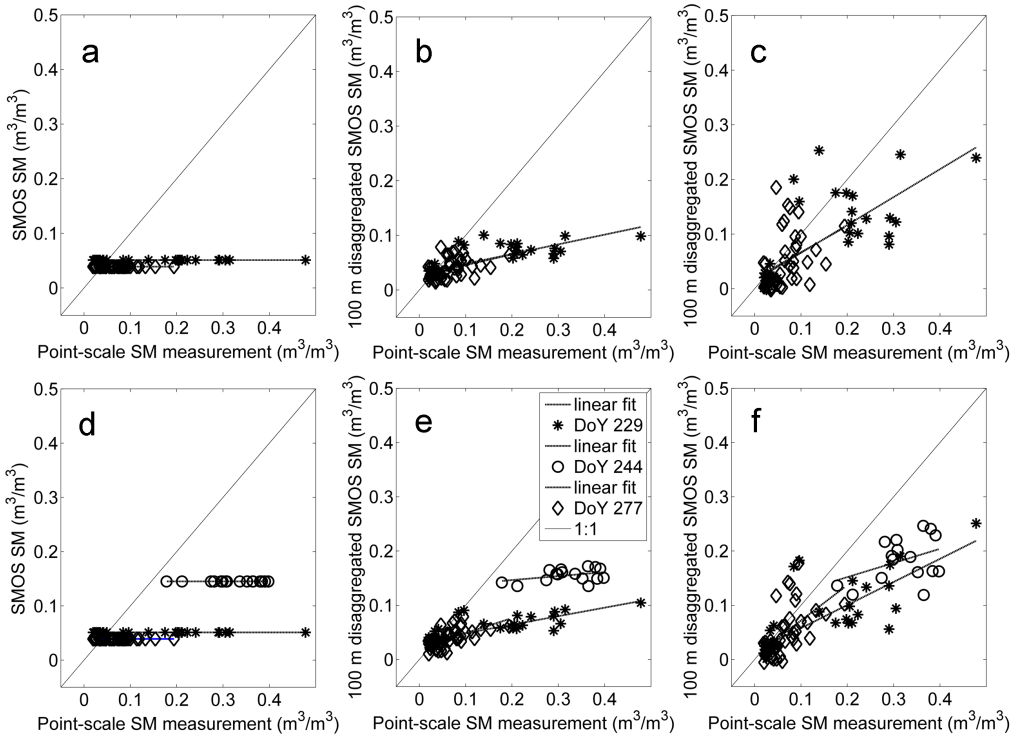

Figure 7: The SMOS soil moisture disaggregated at 100 m resolution in the UNIFORM (a and d), LINEAR (b and e) and NONLINEAR (c and f) mode is plotted as a function of localized situ measurements for ASTER data (top), and Landsat-7 data (bottom). The segments represent the linear fit of daily data.

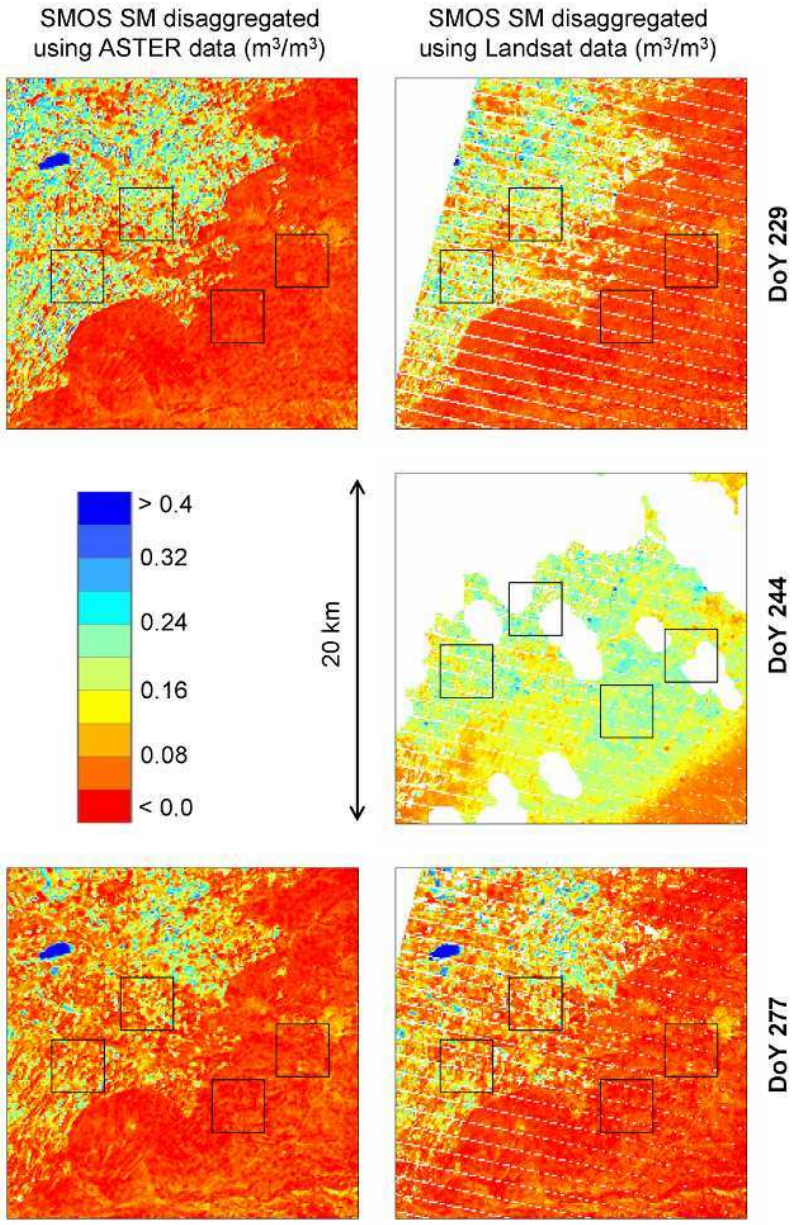

Figure 8: Images of the SMOS data disaggregated at 100 m resolution in NONLINEAR mode using ASTER (left) and Landsat-7 (right) data.

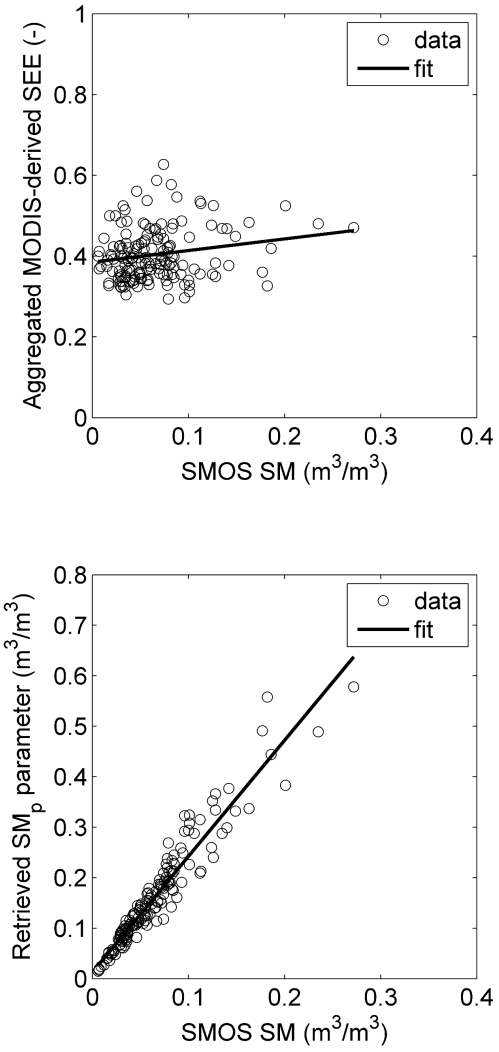

Figure 9: The MODIS-derived SEE aggregated at 40 km resolution (top), and the daily $\mathbf{SM_p}$ parameter retrieved over the study area (bottom) is plotted as a function of SMOS soil moisture for the entire time series spanning from April to October 2011.